

# ChemComm

Accepted Manuscript



This is an *Accepted Manuscript*, which has been through the Royal Society of Chemistry peer review process and has been accepted for publication.

*Accepted Manuscripts* are published online shortly after acceptance, before technical editing, formatting and proof reading. Using this free service, authors can make their results available to the community, in citable form, before we publish the edited article. We will replace this *Accepted Manuscript* with the edited and formatted *Advance Article* as soon as it is available.

You can find more information about *Accepted Manuscripts* in the [Information for Authors](#).

Please note that technical editing may introduce minor changes to the text and/or graphics, which may alter content. The journal's standard [Terms & Conditions](#) and the [Ethical guidelines](#) still apply. In no event shall the Royal Society of Chemistry be held responsible for any errors or omissions in this *Accepted Manuscript* or any consequences arising from the use of any information it contains.



Journal Name

COMMUNICATION

## High Performance Li-ion Sulfur Batteries Enabled by Intercalation Chemistry

Received 00th January 20xx,  
Accepted 00th January 20xx

Dongping Lv<sup>a</sup>, Pengfei Yan<sup>b</sup>, Yuyan Shao<sup>a</sup>, Qiuyan Li<sup>a</sup>, Seth Ferrara<sup>a</sup>, Huilin Pan<sup>a</sup>, Gordon L. Graff<sup>a</sup>, Bryant Polzin<sup>c</sup>, Chongmin Wang<sup>b</sup>, Ji-guang Zhang<sup>a</sup>, Jun Liu<sup>a</sup> and Jie Xiao<sup>a\*</sup>

DOI: 10.1039/x0xx00000x

www.rsc.org/

**The unstable interface of lithium (Li) metal in high energy density Li sulfur (Li-S) batteries raises concerns of poor cycling, low efficiency and safety issues, which may be addressed by using intercalation types of anode. Herein, a new prototype of Li-ion sulfur battery with high performance has been demonstrated by coupling a graphite anode with sulfur cathode (2 mAh cm<sup>-2</sup>) after successfully addressing the interface issue of graphite in ether based electrolyte.**

Sulfur is an attractive cathode candidate for lithium (Li) batteries due to its low cost, high abundance, and 6-10 times higher theoretical capacity than those of the state-of-the-art transition metal oxide and phosphate cathodes.<sup>1-3</sup> Despite these attractive attributes of Li-S batteries, there are many challenges existing in the cathode, electrolyte and anode, which lead to poor cycling stability, low Coulombic efficiency and severe self-discharge.<sup>1, 4, 5</sup> Although thousands of “stable” cycling has been reported in literature for Li-S batteries, thin-film cathode configuration is usually used and uncertainties exist since the mass of cathode and anode are significantly mismatched. When the cathode thickness or sulfur loading is improved to a level close to the practical application, the lithium metal anode always becomes the dominant killing factor due to its continuous evolution into the porous structure.<sup>6</sup> The newly exposed lithium surface is quickly covered by solid electrolyte interface (SEI) e.g. insulating byproducts, building up the cell impedance. In the presence of polysulfides, the impedance increase gets even faster due to the irreversible deposition of polysulfides on the porous lithium thus terminating the cycling quickly.<sup>1, 5, 7, 8</sup> Efforts have been devoted to mitigating the side reactions on lithium metal by using electrolyte additives,<sup>5, 9</sup> surface coating,<sup>10, 11</sup> hybrid lithium anode,<sup>12</sup> additional barrier layers<sup>13</sup> and solid state

electrolyte<sup>14, 15</sup>. Another promising strategy to circumvent these problems is to switch to alternative anodes such as carbon, high capacity Si or Sn.<sup>16-19</sup> However, Si or Sn still undergoes large volume change e.g. instable interface similar as lithium metal.<sup>20</sup> Therefore, the corresponding Li-ion sulfur batteries comprising sulfur and Si (or Sn) show low reversible capacity or poor cycling stability. Recently Brucken *et al.* used hard carbon as the anode in sulfur batteries and greatly improved the cycling stability of cells compared to those with lithium or Si ones.<sup>21</sup> However, cycling reversibility and efficiency as well as side reactions originating from high-surface-area hard carbon itself are still challenging in the long run. Graphite, an intercalation compound, has already been successfully adopted in commercial Li-ion batteries for decades. Compared to conversion-type anode materials or hard carbon, the backbones of layered carbon frameworks have very limited volume change upon Li<sup>+</sup> intercalation/deintercalation and maintain a stable interface on graphite when EC is present, avoiding direct contact between graphite and the electrolyte, which exfoliates graphite layers. These features from graphite are critical to the success of Li-ion batteries and also expect to benefit sulfur batteries since the volume expansion of graphite anode is limited. However, graphite only works well in the presence of EC which forms a protective SEI layer to avoid the continuous co-intercalation of solvent molecules to exfoliate the graphite lattice. Unfortunately, EC is incompatible with polysulfides and/or sulfur radicals generated during cycling of Li-S batteries.<sup>22, 23</sup> That is the reason why most Li-S cells are using ether based solvents such as DOL and 1,2-dimethoxyethane (DME).<sup>24, 25</sup> In this work, we demonstrate that concentrated LiTFSI in DOL enables reversible and stable cycling of graphite in a Li-S system. A proof-of-concept Li-ion sulfur battery with outstanding cycling stability and high energy density has been demonstrated based on a relevant electrode loading of greater than 2.0 mg cm<sup>-2</sup> of sulfur and 2.0 mAh cm<sup>-2</sup> areal capacity.

<sup>a</sup> Electrochemical Materials & Systems Group, Energy & Environment Directorate, Pacific Northwest National Laboratory (PNNL), Richland, Washington 99352, USA.

<sup>b</sup> Environmental Molecular Sciences Laboratory, Pacific Northwest National Laboratory, Richland, WA 99352, USA.

<sup>c</sup> Chemical Sciences and Engineering Division, Argonne National Laboratory, Argonne, Illinois 60439, USA. Email: jie.xiao@pnnl.gov.

† Electronic Supplementary Information (ESI) available: details of Materials synthesis, characterization, electrode preparation, and electrochemical evaluation. See DOI: 10.1039/x0xx00000x

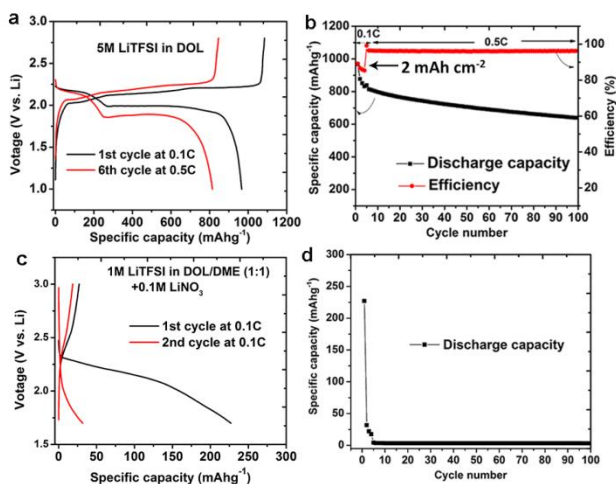


Fig. 1 (a) Charge/discharge curves of LG/S full cell at different C rates in 5M LiTFSI/DOL electrolyte without LiNO<sub>3</sub> and (b) corresponding cycling stability and Coulombic efficiency. (c) Charge/discharge curves of LG/S full cell at 0.1 C in 1M LiTFSI/DOL/DME with 0.1M LiNO<sub>3</sub> as additive and (d) corresponding cycling performance. Areal capacity of cathode is 2 mAh cm<sup>-2</sup>.

Lithiated graphite (LG) has been coupled with a sulfur cathode to construct a full cell by using 5M LiTFSI/DOL as the electrolyte. Promising electrochemical properties are demonstrated from the full cell (LG/S) data in terms of reversible capacity, Coulombic efficiency and cycling stability (Fig. 1a and b). At a low rate of 0.1 C, the LG/S cell exhibits a high capacity of 980 mAh g<sup>-1</sup> (2 mAh cm<sup>-2</sup>) with two flat discharge plateaus at 2.2 and 2.0 V, respectively. This means sulfur in the LG/S full cell experiences similar reaction pathways as those in conventional Li-S cells. In the first charging process, a capacity around 1080 mAh g<sup>-1</sup> is obtained, delivering a high Coulombic efficiency of 90.7% without LiNO<sub>3</sub> additive in the electrolyte. When the rate is elevated to 0.5 C after 5 cycles at 0.1C, a capacity as high as 815 mAh g<sup>-1</sup> is delivered, indicating the good kinetics of Li<sup>+</sup> across the electrolyte, both electrodes and their interfaces. After 100 cycles (Fig. 1b), a high capacity retention of 81.3% can be achieved at 0.5 C with a high Coulombic efficiency of above 97%. DME was removed from the new electrolyte because of the more compatible feature of DOL with the anode.<sup>26, 27</sup> In addition, the LG/S full cell with 5M of LiTFSI in mixed DOL/DME solvents shows inferior cycling performance (Fig. S1). Of note, the cycling performance of full cells also largely depends on the mass balance of the cathode and anode. More systematic optimization is underway to further improve the capacity retention. To our knowledge, this is the first time demonstrating the use of a commercial graphite anode to replace lithium metal for Li-ion sulfur batteries with ether based electrolyte. As a matter of fact, capacity bottleneck of the current state-of-the-art Li-ion batteries is cathode instead of anode (Fig. S2). Therefore, switching from traditional metal oxide cathodes to high capacity sulfur will largely increase the energy density of the whole cell (Table S1).<sup>28</sup> In addition, the use of low-cost sulfur cathode (Table S2) will significantly reduce the cost of the whole system which is one of the main challenges of large scale energy storage technologies.

When traditional electrolyte e.g. 1M LiTFSI in DOL/DME (1:1 v:v) is used, the LG/S full cell cannot be recharged at all (Fig. 1c). Only a small capacity of 220 mAh g<sup>-1</sup> is obtained with a slope during

the first discharge, which is quite different to that of conventional Li-S cells. In the subsequent charging process, there is almost no capacity, indicating the exfoliation of graphite upon Li<sup>+</sup> intercalation which will be discussed in detail in the following part. With repeated cycling, the discharge capacity quickly fades to near zero after only five cycles (Fig. 1d).

Concentrated electrolytes have been reported to reduce the solubility of polysulfides in Li-S batteries, where lithium metal is used as the anode.<sup>7</sup> For comparison, we also tested Li-S cells using a lithium metal anode in 5M LiTFSI/DOL (Fig. S3). However, the cycling is not stable. The reason is because the cathode used in this work, in general, has much higher sulfur mass loading (above 2 mg cm<sup>-2</sup>) than those of most literature reported sulfur electrodes. With the thick cathode configuration, the lithium metal anode also undergoes deep stripping and re-deposition to balance the charge transfer. With that said, the negative effects from the anode will be exacerbated which makes the cycling ability worse than previously reported thin-film Li-S batteries. When graphite is used as the anode, however, the cycling becomes much more stable, confirming that in the cells constructed from sufficiently thick electrodes, the failure factor moves to the anode side with cycling.

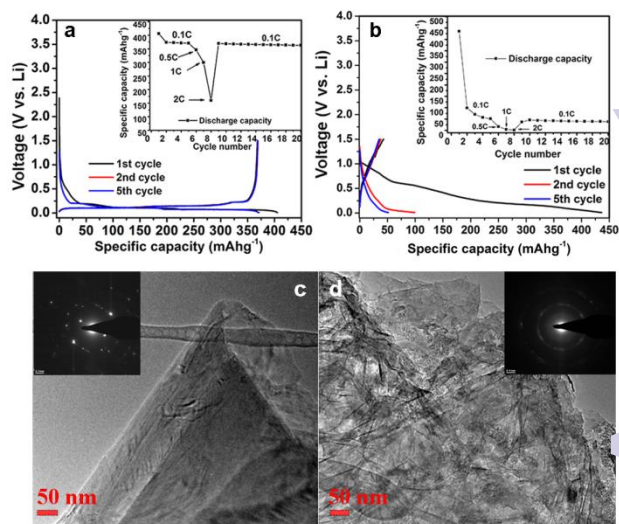


Fig. 2 (a) Charge/discharge curves of Li/G half cell with 5M LiTFSI/DOL electrolyte at 0.1C and corresponding cycling performance (Insert). (b) Charge/discharge curves of Li/G in 1M LiTFSI/DOL/DME electrolyte at 0.1C and corresponding cycling performance (insert). (c) TEM image of the graphite after cycled in (a) for 5 cycles and corresponding ED pattern (insert), and (d) TEM image of the graphite after cycled in (b) for 5 cycles and corresponding ED pattern (insert).

The successful utilization of graphite as the anode for sulfur batteries with ether based electrolyte may be due to the following reasons: (1) maintenance of the layered structure of graphite in the concentrated electrolyte upon charge/discharge, which provides high capacity and reversible Li ion storage and (2) stabilized graphite interface, which suppresses continuous exposure of new surface areas towards the "corrosive" electrolyte as observed in lithium metal anodes in Li-S cells.

To prove the above hypothesis and understand the roles of electrolyte underlying the full cell performances shown in Fig. 1, the electrochemical properties of graphite in the aforementioned different electrolytes are further investigated by using lithium as

the counter electrode. In 5M LiTFSI/DOL electrolyte, graphite exhibits high capacities of 400 and 370 mAh g<sup>-1</sup> at 0.1C for the first discharge and charge processes, respectively (Fig. 2a). Stable capacities around 370 mAh g<sup>-1</sup> are maintained well with high Coulombic efficiency of over 99% in the subsequent cycles. At increased rates of 0.5C, 1C and 2C, graphite still shows high capacities of 320, 280, and 150 mAh g<sup>-1</sup>, respectively. Clear multiple-stage Li<sup>+</sup> intercalation/deintercalation curves are observed within 0.01-0.5 V, and overlap well upon repeated cycling, indicating low electrochemical polarization and high reversibility of graphite. Beyond the voltage range of 0.01-0.5 V, little reduction or oxidation of the electrolyte is observed. This is different to the behaviors of graphite in EC contained electrolyte, where the reduction of the conventional electrolyte happens at 0.7-0.9V in the first cycle and forms protective SEI on graphite.<sup>24, 29</sup> In the case of 1M LiTFSI/DOL/DME, however, graphite shows very poor electrochemical properties in terms of both reversible capacity and cycling stability. As shown in Fig. 2b, significant reduction plateaus at 0.80 and 0.5 V are observed, which are ascribed to the co-intercalation and followed decomposition of solvent. As a result, the first discharge and charge capacities are ca. 450 and 50 mAh g<sup>-1</sup>, respectively, with a very low Coulombic efficiency of 11.1%. Upon cycling, only very limited capacities are obtained at 0.1 C or higher C rates, indicating quick failure/exfoliation of the graphite electrode. Similarly, when graphite is cycled in 1M LiTFSI/DOL electrolyte by excluding DME as a solvent, big irreversible capacity is still found in the first cycle (Fig. S4), indicating low stability of graphite in relatively diluted ether based electrolyte. Transmission electron microscopy (TEM) is used to unravel the mechanism behind different electrolytes. After 5 cycles in 5M LiTFSI/DOL, smooth surface and well maintained graphite particles were found (Fig. 2c). The electron diffraction (ED) result indicates nice crystallinity of graphite (Fig. 2c insert), confirming the high stability of graphite lattice after cycling in the concentrated ether-based electrolyte, consistent with the electrochemical performance in Fig. 2a. Fig. 2d compares graphite morphology after 5 cycles in 1M LiTFSI/DOL/DME electrolyte. Graphite particles are significantly exfoliated (Fig. 2d) and transformed into amorphous plates as demonstrated by ED (Fig. 2d insert). It is exceptional that no obvious SEI layer or surface depositions are observed on the surface of graphite cycled in concentrated electrolyte. For comparison, we also test graphite in the traditional EC-containing electrolyte (1M LiPF<sub>6</sub>/EC/EMC) at exactly the same experimental conditions. Clear SEI with ca.10 nm thickness is observed on the surface of graphite (Fig. S5). These results indicate that the functioning mechanism of concentrated LiTFSI in pure DOL is quite different with that of the traditional EC-based electrolytes. More investigation is underway now to further understand the protection mechanism of the graphite surface in concentrated LiTFSI/DOL electrolyte, which will be published soon elsewhere.

Another question that needs to be answered is the interface stability of graphite in the presence of polysulfides. Polysulfides are "corrosive" and continuously consume Li metal in traditional Li-S cells. As a result, the surface area of Li anodes will keep growing, which builds up electrode interfacial resistance. For comparison, the interfacial properties of graphite are studied after being cycled in LG/S full cell. As shown in Fig. 3, after 100 cycles the graphite

electrode shows similar morphology as the pristine one (Fig. 3a), without any observation of surface cracks or exfoliation (Fig. 3a and b), indicating high stability of the graphite structure upon cycling. Cross-sectional scanning electron microscopy (SEM) image (Fig. 3c) of the cycled graphite electrode demonstrates that the electrode expands slightly from 53  $\mu\text{m}$  to 63-74  $\mu\text{m}$ . Electrode expansion is common due to the swell of either active material or binder when contacting with electrolyte. It is interesting to find that the bulk graphite as well as its interface is quite stable upon cycling. Fig. 3d exhibits a cross-sectional image of a single graphite particle by focused ion beam (FIB)-SEM. The particle shows a solid dark core with a thin layer of coating outside (ca. 100-200 nm). The EDX analysis (Fig. 3e-f) is performed at the very surface and core area of the selected particle. It is clear that the core of graphite is carbon majority with a trace of residual oxygen. The surface layer is coated by the byproducts from polysulfide depositions. Electrolyte decomposition also contributes to the surface layer coating but is not a major component, consistent with the almost invisible SEI in Fig. 2c. This means graphite interface is stable enough to endure the attack from polysulfides and maintains its structure integrity. Therefore, the irreversible loss of polysulfides and SEI accumulation on the anode side are both alleviated, which greatly improves the cycling stability of the Li-ion sulfur cell. To further confirm the effectiveness of the graphite anode in promoting the cycling ability of Li-ion sulfur cells, Li and graphite anodes harvested from cycled Li-S and Li-ion sulfur cells (at charged state), respectively, are immersed in the DOL/DME mixture solvent. It is interesting to see that the solution containing cycled Li anode changes to yellow immediately, while the one with cycled graphite remains nearly colorless (Fig. S7). These results further indicate that sulfur species "leaked" out of the cathode side easily accumulate on the porous lithium metal anode during cycling.<sup>6</sup> The anode contamination should be one of the major reasons for capacity decay in Li-S batteries, which has been significantly suppressed by using a graphite anode.

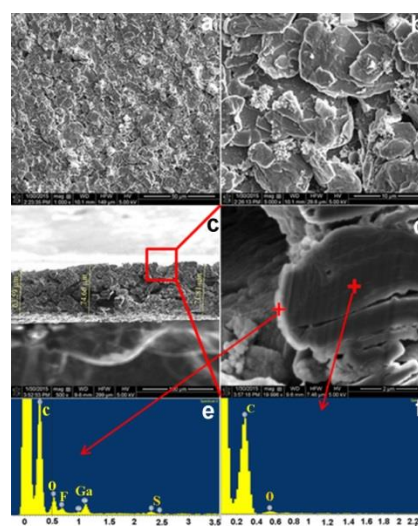


Fig. 3 (a) SEM images of graphite electrode after 100 cycles in LG/S full cell with 5M LiTFSI/DOL electrolyte. (b) Magnification of (a). (c) Cross-sectional SEM image of cycled graphite anode. (d) FIB-SEM cross-sectional image of a single graphite particle in (c). (e) and (f) Point EDS at the very edge and core area of the graphite particle in (d), respectively.

In summary, the strategy of using intercalation anode to address the key issues associated with conventional Li-S batteries has been successfully demonstrated by constructing a Li-ion sulfur battery employing graphite as the anode. Without any additive, the LG/S full-cell with sulfur loading  $>2 \text{ mg cm}^{-2}$  delivers a high reversible capacity of  $980 \text{ mAh g}^{-1}$  and a capacity retention of 81.3% along with a high efficiency of above 97% after 100 cycles, simply by increasing the concentration of LiTFSI solute to 5M in pure DOL solvent. It is revealed that the interface property of the graphite anode in concentrated LiTFSI/DOL has been drastically changed, forming a very thin and almost invisible SEI to protect the graphite lattice. This study may provide new insights for developing high performance sulfur batteries coupled with versatile anode materials to remove the lithium metal issues in the system.

This work was fully supported by the Assistant Secretary for Energy Efficiency and Renewable Energy, Office of Vehicle Technologies of the U.S. Department of Energy (DOE) under Contract No. DEAC02-05CH11231 for PNNL and under DEAC02-98CH10886 under the Battery Materials Research (BMR) program. The XPS and TEM characterization were conducted in the William R. Wiley Environmental Molecular Sciences Laboratory (EMSL)—a national scientific user facility located at PNNL which is sponsored by the DOE's Office of Biological and Environmental Research (BER). PNNL is operated by Battelle for the DOE under Contract DE-AC05-76RLO1830.

#### Notes and references

1. P. G. Bruce, S. A. Freunberger, L. J. Hardwick and J.-M. Tarascon, *Nat. Mater.*, 2012, **11**, 19-29.
2. M. S. Whittingham, *Chem. Rev. (Washington, DC, U. S.)*, 2004, **104**, 4271-4301.
3. J. M. Tarascon and M. Armand, *Nature*, 2001, **414**, 359-367.
4. X. Ji and L. F. Nazar, *J. Mater. Chem.*, 2010, **20**, 9821-9826.
5. D. Aurbach, E. Pollak, R. Elazari, G. Salitra, C. S. Kelley and J. Affinito, *J. Electrochem. Soc.*, 2009, **156**, A694-A702.
6. D. Lv, J. Zheng, Q. Li, X. Xie, S. Ferrara, Z. Nie, L. B. Mehdi, N. D. Browning, J.-G. Zhang, G. L. Graff, J. Liu and J. Xiao, *Adv. Energy Mater.*, 2015, DOI: 10.1002/aenm.201402290.
7. L. Suo, Y.-S. Hu, H. Li, M. Armand and L. Chen, *Nat. Commun.*, 2013, **4**.
8. D. Lv, Y. Shao, T. Lozano, W. D. Bennett, G. L. Graff, B. Polzin, J. Zhang, M. H. Engelhard, N. T. Saenz, W. A. Henderson, P. Bhattacharya, J. Liu and J. Xiao, *Adv. Energy Mater.*, 2015, **5**, 1400993.
9. Z. Lin, Z. Liu, W. Fu, N. J. Dudney and C. Liang, *Adv. Funct. Mater.*, 2013, **23**, 1064-1069.
10. S. S. Zhang and J. A. Read, *J. Power Sources*, 2012, **200**, 77-82.
11. R. Demir-Cakan, M. Morcrette, Gangulibabu, A. Gueguen, R. Dedryvere and J.-M. Tarascon, *Energy & Environ. Sci.*, 2013, **6**, 176-182.
12. C. Huang, J. Xiao, Y. Shao, J. Zheng, W. D. Bennett, D. Lu, L. V. Saraf, M. Engelhard, L. Ji, J. Zhang, X. Li, G. L. Graff and J. Liu, *Nat Commun*, 2014, **5**.
13. Y.-S. Su and A. Manthiram, *Nat. Commun.*, 2012, **3**.
14. Z. Lin, Z. Liu, W. Fu, N. J. Dudney and C. Liang, *Angewandte Chemie International Edition*, 2013, **52**, 7460-7463.
15. A. Hayashi, T. Ohtomo, F. Mizuno, K. Tadanaga and M. Tatsumisago, *Electrochem. Commun.*, 2003, **5**, 701-705.
16. Y. Yang, M. T. McDowell, A. Jackson, J. J. Cha, S. S. Hong and Y. Cui, *Nano Letters*, 2010, **10**, 1486-1491.
17. M. Agostini, J. Hassoun, J. Liu, M. Jeong, H. Nara, T. Momma, T. Osaka, Y.-K. Sun and B. Scrosati, *ACS Applied Materials & Interfaces*, 2014, **6**, 10924-10928.
18. J. Hassoun and B. Scrosati, *Angewandte Chemie-International Edition*, 2010, **49**, 2371-2374.
19. W. Zhou, X. Xiao, M. Cai and L. Yang, *Nano Letters*, 2014, **14**, 5250-5256.
20. C.-M. Park, J.-H. Kim, H. Kim and H.-J. Sohn, *Chem. Soc. Rev.*, 2010, **39**, 3115-3141.
21. J. Brückner, S. Thieme, F. Böttger-Hiller, I. Bauer, H. T. Grossmann, P. Strubel, H. Althues, S. Spange and S. Kaskel, *Adv. Funct. Mater.*, 2014, **24**, 1284-1289.
22. Q. Wang, J. Zheng, E. Walter, H. Pan, D. Lv, P. Zuo, H. Chen, Z. D. Deng, B. Y. Liaw, X. Yu, X. Yang, J.-G. Zhang, J. Liu and J. Xiao, *J. Electrochem. Soc.*, 2015, **162**, A474-A478.
23. M. Cuisinier, C. Hart, M. Balasubramanian, A. Garsuch and L. F. Nazar, *Adv. Energy Mater.*, 2015, DOI: 10.1002/aenm.201401801, n/a-n/a.
24. D. Aurbach, B. Markovsky, I. Weissman, E. Levi and Y. Ein-Or, *Electrochim. Acta*, 1999, **45**, 67-86.
25. J. O. Besenhard, M. Winter, J. Yang and W. Biberacher, *J. Power Sources*, 1995, **54**, 228-231.
26. Y. V. Mikhaylik, I. Kovalev, R. Schock, K. Kumaresan, J. Xu and J. Affinito, *ECS Trans.*, 2010, **25**, 23-34.
27. V. Etacheri, U. Geiger, Y. Gofer, G. A. Roberts, I. C. Stefan, R. Fasching and D. Aurbach, *Langmuir*, 2012, **28**, 6175-6184.
28. S. Kaskel, presented in part at the 249th ACS national meeting & exposition, Denver, CO, March 22-26, 2015.
29. D. Aurbach, M. D. Levi, E. Levi and A. Schechter, *J. Phys. Chem. B*, 1997, **101**, 2195-2206.